



ELSEVIER

Contents lists available at ScienceDirect

## Chemical Engineering Science

journal homepage: [www.elsevier.com/locate/ces](http://www.elsevier.com/locate/ces)

# Gas-liquid flow and mass transfer in a microchannel under elevated pressures



Chaoqun Yao<sup>a,b</sup>, Zhengya Dong<sup>a,b</sup>, Yuchao Zhao<sup>a</sup>, Guangwen Chen<sup>a,\*</sup>

<sup>a</sup> Dalian National Laboratory for Clean Energy, Dalian Institute of Chemical Physics, Chinese Academy of Sciences, Dalian 116023, China

<sup>b</sup> University of Chinese Academy of Sciences, Beijing 100049, China

## HIGHLIGHTS

- The sizes of CO<sub>2</sub> bubbles and liquid slugs were determined under different pressures.
- An online method was used to study the bubble dissolution and mass transfer rate.
- $k_1a$  and  $k_l$  increase with the increase in system pressure.
- The maximum dissolution of CO<sub>2</sub> bubbles is linear to the liquid slug size.
- Gas absorption during bubble formation was measured.

## ARTICLE INFO

### Article history:

Received 29 July 2014

Received in revised form

2 October 2014

Accepted 1 November 2014

Available online 10 November 2014

### Keywords:

Taylor flow

Gas-liquid

Carbon dioxide

Microreactor

Dissolution

## ABSTRACT

Flow and mass transfer of gas-liquid slug flow under elevated pressures up to 3.0 MPa in a microchannel are investigated with CO<sub>2</sub>-water system. The results show that the ratio of the initial bubble length to the unit cell length is linear with the injection gas volume fraction under each pressure condition, but the slope decreases with an increase in the system pressure. The mass transfer coefficients are calculated with a unit cell model based on the dissolution rate of gas bubbles. Increasing pressure leads to larger mass transfer coefficients, as well as higher amount of gas absorption during the bubble formation. But the fraction of gas absorption during the bubble formation stage is only about 1.5~4.0% of feeding gas. For the bubble dissolution in the main channel, the dissolution rates at different flow rates differ very little for short contact distances from the T-junction, whereas the balance limitation of dissolution at large contact distances only depends on the amount of liquid in a unit cell.

© 2014 Elsevier Ltd. All rights reserved.

## 1. Introduction

Microreaction technology holds great promises for process intensification in diverse chemical engineering applications due to the capabilities of providing high mass and heat transfer rate, improved process control and overall equipment size reduction (Chen et al., 2008; Jensen, 2001). These merits make the implementation of this technology much safer in practice because of not only its excellent thermal management (Chao et al., 2009, 2010), but also low material hold-up. Moreover, the numbering-up methodology for its production throughput increase largely reduces the time from lab research to industrial application.

With controllable and very high specific surface area, microreactors are especially suitable for multiphase processes. For gas-liquid two-phase systems, such as absorption (Ye et al., 2013) and reaction

(Keybl and Jensen, 2011; Trachsel et al., 2008; Zhao et al., 2013b), many researches have shown that microreactors have great advantages (Hessel et al., 2005). Generally, gas-liquid two-phase flow patterns in microchannels include bubbly, slug, unstable slug, slug-annular, annular and churn flows (Shao et al., 2009; Triplett et al., 1999). Among these flow patterns, slug flow is the most studied one due to its remarkable features. It is dominant under wide operating conditions with regular dispersion of gas bubbles and liquid slugs. The gas bubble and liquid slug move alternatively in the channel, rendering low back mixing and narrow residence time distribution. A large surface area, along with the inner recirculation in the liquid slug, makes it possibly to substantially improve heat and mass transfer processes. (Zaloha et al., 2012). Therefore, slug flow appears to be a very promising operational mode for the intensification of gas-liquid reactions.

Gas-liquid mass transfer within a slug flow mainly contains two zones: (1) between bubble caps and the neighboring liquid slugs and (2) between the bubble body and the adjacent liquid film around the channel wall (Sobieszuk et al., 2012; van Baten

\* Corresponding author. Tel.: +86 411 8437 9031; fax: +86 411 8469 1570.

E-mail address: [gwchen@dicp.ac.cn](mailto:gwchen@dicp.ac.cn) (G. Chen).

and Krishna, 2004), as shown in Fig. 1. The first mass transfer zone is closely related to the mixing in the liquid slug due to recirculation (Zaloha et al., 2012), whereas the latter one is affected largely by the effectiveness of the liquid film (Pohorecki, 2007). For example, when very long bubbles are generated, the liquid film can be easily saturated and becomes ineffective due to long gas-liquid contact time. Mass transfer in the above two zones will increase with increasing flow rates because of higher surface renewal rates. As a result, the overall mass transfer performance depends on many factors, such as bubble length, slug length and bubble velocity, etcetera. The overall mass transfer performance is also affected by the mixing in the liquid phase, which generally occurs between the liquid slug and the liquid film. It favors high bubble velocity, and can also be enhanced by channel bends and special inner channel structures (Muradoglu, 2010; Su et al., 2009; Zaloha et al., 2012). Up to now, many researches have been devoted to the mass transfer characteristics of slug flow (Berčić and Pintar, 1997; Ganapathy et al., 2013; Sobieszuk et al., 2011; Vandu et al., 2005; Yue et al., 2009). However, the existing studies are all under atmospheric conditions, which do not represent the real conditions in the majority of gas-liquid reactions in the chemical industry.

It is well known that high pressure is beneficial for gas-liquid reactions due to the increase of gas solubility in the liquid phase and feed throughput for the same reactor size. Many studies have already been focused on developing applications of high-pressure microfluidics (Keybl and Jensen, 2011; Marre et al., 2010; Trachsel et al., 2008; Verboom, 2009). But the design is usually arbitrary. Therefore, there is a growing need to study the transport phenomena involved in gas-liquid processes in microchannels. Zhao et al. (2013a) studied the gas-liquid flow patterns under elevated pressures up to 5.0 MPa. They found a shift of transition line between bubbly and slug flows to higher gas-phase Weber number and low liquid-phase Weber number when system pressure is elevated. Yao et al. (2014a) investigated the effect of system pressure on gas-liquid slug flow. A strong leakage flow was found to increase with the increase in system pressure, leading to a bubble formation shift from the transition regime to the squeezing regime. Apart from these studies, there is still a lack of detailed knowledge about the transport phenomena under different pressures in microchannels, especially concerning the gas-liquid mass transfer characteristics.

The present work aims at improving the fundamental understanding into gas-liquid flow and mass transfer under elevated pressures. Taylor flow of CO<sub>2</sub>-H<sub>2</sub>O mixture was investigated, where flow characteristics such as bubble and slug lengths were measured by imaging method. And mass transfer information was extracted from the dissolution of CO<sub>2</sub> bubbles. Finally, mass transfer coefficients and the amount of absorption during bubble formation were calculated and compared under different system pressures up to 3.0 MPa.

## 2. Experimental section

### 2.1. Microchannel devices

Fig. 2 shows the schematic diagram of the gas-liquid microchannel contactor used in this study. Gas-liquid slug flow was generated at the T-junction and moved downstream the channel.

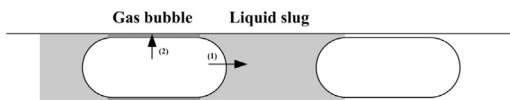


Fig. 1. Mass transfer in the gas-liquid slug flow.

The contactor module was composed of transparent polyaryl sulfone (PASF), polycarbonate (PC) and stainless steel materials. The channel with a cross section of 600  $\mu\text{m} \times 300 \mu\text{m}$  (width  $\times$  depth) was fabricated on a PASF substrate by using milling technology. The machined PASF plate was covered by another smooth PASF plate. The two plates were sandwiched by two PC plates, then by two stainless steel plates. With steel screws, the microchannel contactor was tightly sealed so that no leakage occurred at 5 MPa gas-tightness experiments. The contactor houses an observation window that enabled complete record of flow patterns in the meandering microchannel.

### 2.2. Experimental setup

Pure CO<sub>2</sub> and deionized water were used as test fluids to study the flow and mass transfer under elevated pressures. The experimental setup was shown in Fig. 3. CO<sub>2</sub> was provided from a cylinder and controlled by a series of mass flow controllers with different flow ranges (D07-7B, Beijing Seven Star Electronics, China, accuracy of 0.5% full scale). Deionized water was pumped by a high-precision digital piston pump (Beijing Satellite Manufacturing Factory, measurement range: 0~5 mL/min, precision: 0.3%). The system pressure was

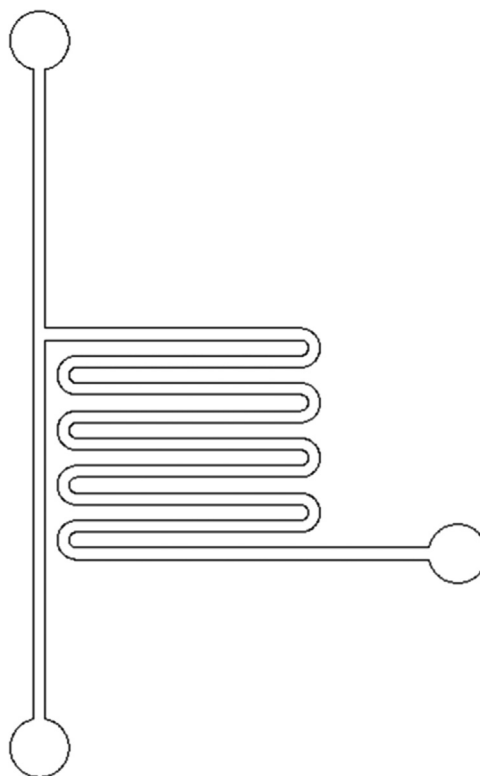


Fig. 2. Schematic diagram of the gas-liquid microchannel contactor.

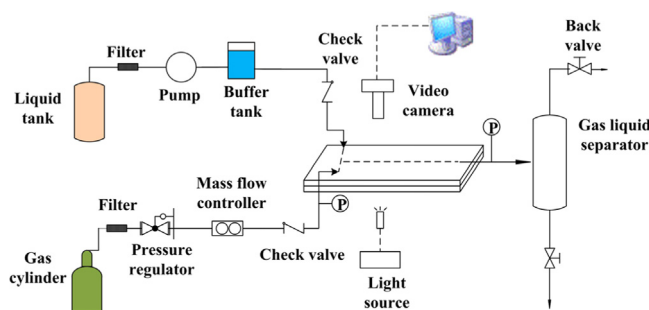


Fig. 3. Schematic of the experimental setup.

regulated by a back pressure valve. Gas flow rates were calibrated before experiments while the liquid flow rates were measured under each run. The pressures at the gas phase inlet and at the gas-liquid mixture outlet were measured with two pressure transducers, thus the pressure drop of the flow in the channel could be determined. All experiments were conducted under room temperature.

In the experiments, the system pressure ranged from 0.1 to 3.0 MPa. It is important to note that the gas flow rates mentioned in this article are all based on the volumetric rates. This means that the gas mass flow rates increase with the increase in pressure. All the parameters defined are based on the inlet condition due to the gas flow rates decrease in the channel through absorption.

### 2.3. Methodology for the determination of mass transfer coefficients

Because the system pressure is regulated by a back pressure valve after the gas-liquid separator, the end effects cannot be eliminated, including absorption in the inlet junction, outlet tube and the separator. Therefore, the determination of mass transfer performance in microchannels under elevated pressure is very difficult by offline methods, which usually involve analyzing the components in the outlet gas or liquid phase. In this work, the mass transfer coefficients were calculated with an online method developed in our previous work (Yao et al., 2014b). The slug flow patterns were recorded by a high speed camera system. Flow details such as gas bubble length, liquid slug length and bubble velocity can be obtained from the captured images. Since CO<sub>2</sub> has a relatively large solubility in water, the detectable decrease of bubble volume appears when bubble moves downstream the channel. Therefore, with a unit cell model, the absorption rate and the mass transfer coefficients were determined based on the shrinkage of bubble length. A schematic description of the unit cell model is shown in Fig. 4.

The model is based on the following assumptions:

1. In each unit cell, gas and liquid phases are both well mixed, respectively.
2. Mass transfer from gas to liquid phase only happens in single unit cell.
3. No mixing happens between different unit cells.
4. Bubble shape in the cross-section doesn't change if bubble length is large enough

With these assumptions, when a unit cell moves forward, mass balance of CO<sub>2</sub> between gas phase and liquid phase in the unit cell can be expressed as

$$\frac{dV_B}{dt} = \frac{dV_B}{dx} U_B = -k_L a (C^* - C) V_L \frac{RT}{P} \quad (1)$$

where  $V_L$  and  $V_B$  denote the volume of liquid and gas bubble in single unit cell,  $U_B$  the bubble moving velocity,  $C$  the CO<sub>2</sub> concentration in liquid phase and  $k_L a$  the liquid side volumetric mass transfer coefficient. As indicated by Berčić and Pintar (1997) and Yue et al. (2007), the relationship between CO<sub>2</sub> concentration in water and distance from the inlet junction in a microchannel is

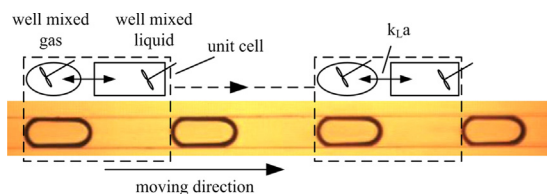


Fig. 4. Schematic representation of the unit cell model.

calculated as

$$C^* - C = (C^* - C_0) e^{-(x/j_L)k_L a} \quad (2)$$

where  $C_0$  is the liquid concentration at  $x_0$  and equals 0 if  $x_0$  is at the T-junction where gas and liquid starts to contact.  $j_L$  represents the liquid superficial velocity. The last assumption is well satisfied if bubble length is much larger than the channel width, for example, 1.2 W. Under this condition, bubble volume shrinkage can be treated to be linear with its length reduction, thus,  $dV_B/dx = A_B dL_B/dx$ . Substituting this relationship and Eq. (2) into Eq. (1) and replacing the bubble velocity with the logarithm average bubble velocity, we can obtain a solution of Eq. (1) by integrating from  $x_0$  to  $x$  as

$$L_B = L_{B0} - \frac{C^* - C_0}{U_B A_B} V_L \frac{RT}{P} j_L (1 - e^{-(x/j_L)k_L a}) \quad (3)$$

where  $L_B$  denotes bubble length at a distance of  $x$  and  $L_{B0}$  denotes bubble length at  $x_0$ . It should be noted that when  $x_0$  equals 0,  $L_{B0}$  is a virtual parameter representing length of gas bubble right at the T-junction as there is no true complete bubble there. This approach was reasonable for  $L_{B0}$  of CO<sub>2</sub> bubble that was nearly equal to the length of N<sub>2</sub> bubble formed under similar flow conditions as indicated in our previous study (Yao et al., 2014b). Eq. (3) indicates that the relationship between bubble length and their location follows an exponential type:

$$L_B = m_1 + m_2 e^{-m_3 x} \quad (4)$$

where

$$m_1 = L_{B0} - \frac{C^* - C_0}{U_B A_B} V_L \frac{RT}{P} j_L \quad (5)$$

$$m_2 = \frac{C^* - C_0}{U_B A_B} V_L \frac{RT}{P} j_L \quad (6)$$

The physical meaning of  $m_1$  is the final bubble length when the liquid phase is saturated and the meaning of  $m_2$  is the corresponding gas bubble length of the liquid absorption capacity in a unit cell. By fitting the bubble length at different locations, the liquid side volumetric mass transfer coefficient  $k_L a$  can be determined. Fig. 5 shows a typical image of bubble shrinkage and calculation of mass transfer coefficient with the unit cell model. Another prerequisite to use this method is that the pressure drop should be small enough, so that the effect on the bubble expansion is negligible. Therefore, liquid and gas flow rates were carefully chosen to satisfy this prerequisite. More detailed information about this online method including bubble expansion evaluation, model description and validation can be found in Yao et al. (2014b).

## 3. Results and discussion

### 3.1. Initially generated gas bubble and liquid slug lengths

The slug flow is mainly characterized by the lengths of gas bubbles and liquid slugs. They are very important parameters for determining mass and heat transfer performance. The initially generated bubble length is defined as the length of bubbles that obtain their regular shapes right after generation. Herein in this article, it is referred as  $L_{B1}$ . Fig. 6 shows the evolution of initial bubble and slug length as a function of gas-liquid flow ratio under different system pressures. It shows that higher inlet gas flow rate results in longer gas bubbles and shorter liquid slugs. For a given liquid flow rate, the bubble length linearly scales with the gas flow rate, which corresponds to the well-known Garstecki model (Garstecki et al., 2006). On the other hand, the liquid slug length is inversely proportional to gas flow rate. Unlike the effect of flow rates, the effect of system pressure on the bubble and slug length is much more complicated. In the present study, it was observed

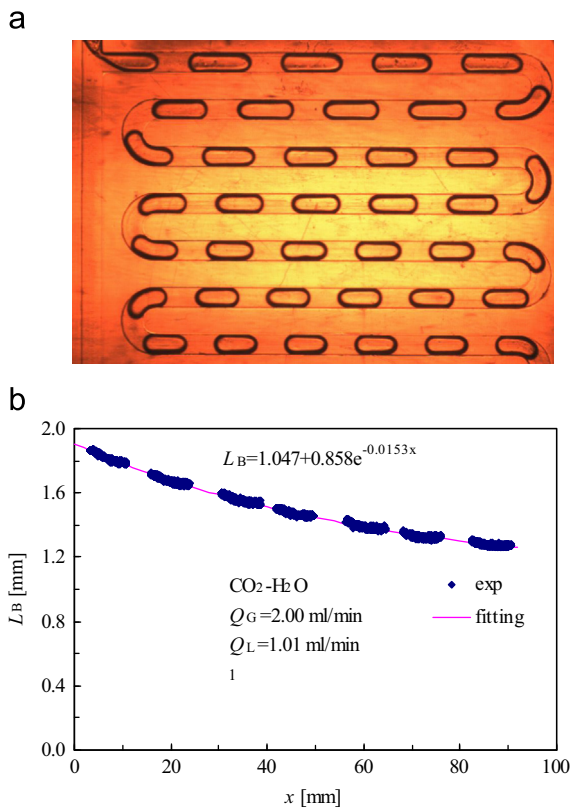


Fig. 5. Exemplary showing of the (a) mass transfer process and (b) data fitting.

that increasing the system pressure generally led to a shorter generated gas bubble, as shown in Fig. 6(a). It was different from  $N_2$ - $H_2O$  system, where an inconspicuous effect of system pressure was observed (Yao et al., 2014a). This may result from several reasons. Firstly, much lower  $CO_2$ - $H_2O$  interfacial tension is obtained at higher pressure (dos Santos and Levin, 2010; Nielsen et al., 2012), which leads to a faster bubble rupture process. Secondly, gas bubble has a larger cross-sectional area at higher pressure (Yao et al., 2014a), resulting in smaller bubble lengths for a fixed gas bubble volume. For  $CO_2$ - $H_2O$  system, more gas was absorbed during the bubble formation under higher pressure conditions, which will be discussed in the following sections of the article. As a result, smaller bubbles were generated. However, when the system pressure is further elevated to 3.0 MPa, the effect of increase in gas density dominates and leads to a slower bubble rupture. Therefore, bubble length increases at 3.0 MPa. The effect of system pressure on the liquid slug length is not obvious, since many other factors affected by system pressure such as the liquid film thickness, leakage flow and generation frequency, also have a large influence on the slug length (van Steijn et al., 2007; Yao et al., 2013). The complex interaction among these factors leads to an unclear effect of system pressure on the slug length.

A precise prediction of bubble and slug lengths in microchannels is still a difficult task despite that many efforts have been devoted to this. In this study, the capillary number was close to 0.01, which is generally treated to be the critical value of bubble pinch-off regime between squeezing and shearing (de Menech et al., 2008; Garstecki et al., 2006; Guo and Chen, 2009). So the bubble formation here is likely to be in the transition regime. Although interfacial tension still dominates under these conditions, shear stress and resistance force also play important roles in the bubble formation process, which makes it very difficult to predict the bubble and slug length. Thus, taking a step back to only characterizing the volume fraction of each phase is much easier.

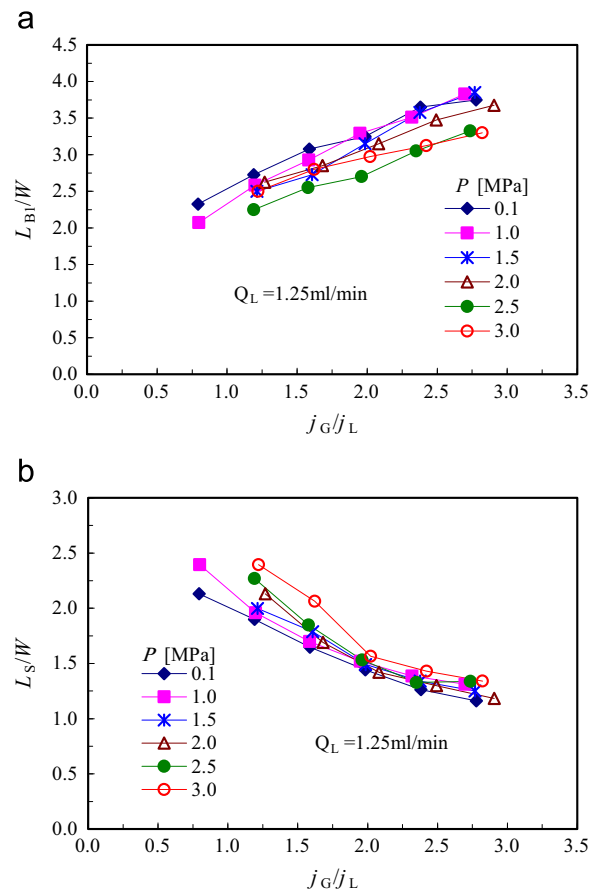


Fig. 6. Evolution of (a) dimensionless initially generated bubble length and (b) dimensionless slug length versus gas-liquid superficial velocity ratio under different system pressures. The superficial velocity is defined as volumetric flow rate divided by the cross sectional area of the channel.

Here, a simple parameter  $L_{B1}/(L_{B1}+L_S)$  is used to describe the volume fraction. The results plotted as a function of the injection volume fraction  $j_G/(j_G+j_L)$  is presented in Fig. 7, which nicely correlates with the expression

$$\frac{L_{B1}}{L_{B1}+L_S} = \beta \frac{j_G}{j_G+j_L} \quad (7)$$

The constant  $\beta$  equals 1.051 at atmospheric pressure and decreases with the increase of system pressure, as shown in Fig. 7(c). The result clearly indicates that smaller gas bubbles were generated at higher system pressure, as stated before.

### 3.2. Dissolution rate

Dissolution rate of gas bubbles is very important to evaluate the reactor performance for gas absorption. Fig. 8(a) shows the evolution of gas bubble length at five different gas flow rates. The solid lines represent the fitted data using Eq. (4) for better visualization. As expected, longer bubbles were obtained at larger gas flow rates. The dissolution rate of single bubbles, however, seemed to be insignificantly affected by gas flow rates as the curves appeared parallel. In fact, the mass transfer rate was larger at higher flow rates. The dissolution rate should deviate a lot if it is plotted as a function of time. But as a function of channel length, the amount of gas absorbed for short contact distances (e.g. < 40 mm) was very close for different conditions, as shown in Fig. 8(b). This fact was in accordance with the findings of Zalloha et al. (2012). They found that the product of the inner recirculation rate inside the liquid slug and the residence time was independent

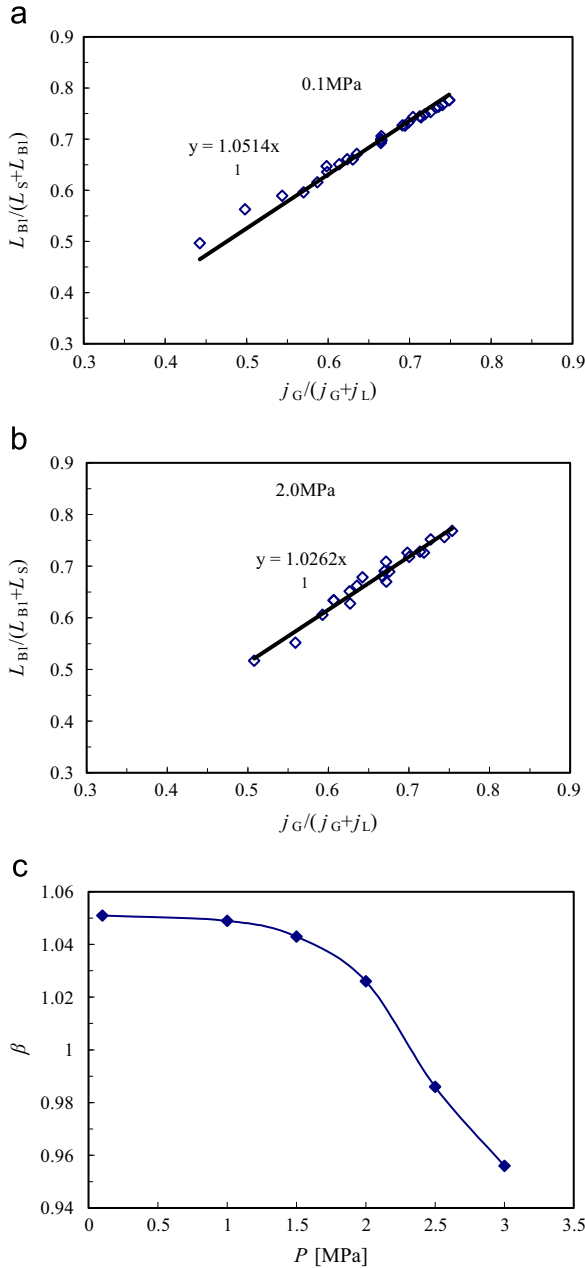


**Fig. 7.** Initial gas-liquid flow arrangement. (a) and (b) Exemplary showing of the linear relationship between  $L_{B1}/(L_{B1}+L_S)$  and injection gas volume fraction  $j_G/(j_G+j_L)$  at 0.1 and 2.0 MPa, respectively. (c) Slopes of the linear relationship as a function of system pressure.

of total superficial velocity, which means that the product of mass transfer rate ( $k_L a$ ) and mass transfer time is constant. For short contact distances, with negligible difference in the solute concentration driving force, the bubble size reduction had no significant difference. As the solute concentration in liquid phase increases with bubbles moving further downstream, leading to a slowed-down dissolution rate ( $k_L a(C^b-C)$ ), the deviation in the amount of absorbed gas becomes larger at larger distances, as shown in Fig. 8(b).

Fig. 8(b) also shows that a larger gas flow rate leads to a smaller  $L_{B0}-L_B$  at final stage. In fact, not only increasing gas flow rates but also increasing liquid flow rates could result in similar phenomenon. The reason is that shorter liquid slugs are generated under these conditions as discovered in previous articles (Yao et al., 2014a, 2013). From the above analysis, one can conclude that the amount of finally absorbed gas in single unit cell only depends on

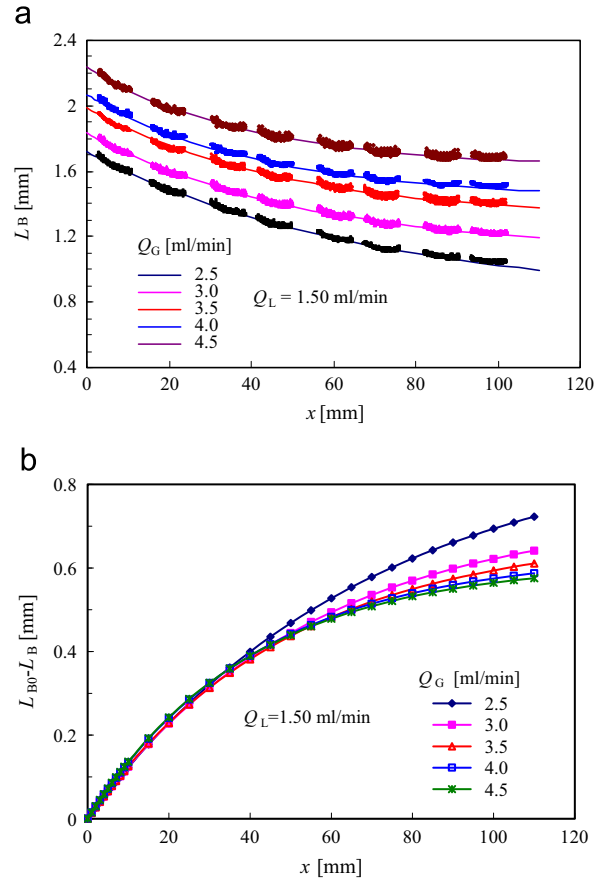


**Fig. 8.** Evolution of (a) gas bubble length (b) bubble absorption along microchannel at  $Q_L=1.50$  ml/min and  $P=0.1$  MPa.

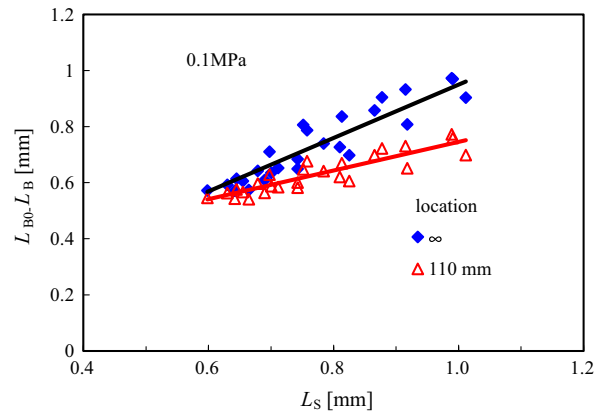


**Fig. 9.** Linear relationship between liquid slug length and bubble size reduction at 110 mm and infinity,  $P=0.1$  MPa.

the amount of liquid in the unit cell (Zaloha et al., 2012). The conclusion is verified by the plotting in Fig. 9. As can be seen,  $L_{B0}-L_B$  near the outlet at about a distance of 110 mm from the T-junction linearly scales with the liquid slug length. A larger slug length results in larger gas absorption due to the higher absorption capacity. Since the bubble size  $L_B$  as a function of the distance  $x$  can be excellently described by Eq. (4),  $L_{B0}-L_B$  at infinity can be extrapolated as  $m_2$  of which the physical meaning is the maximum amount of gas absorption in single unit cell. Similarly, a linear relationship between  $m_2$  and  $L_S$  is obtained. A little deviation of the data is due to other contributions from the flow of liquid around gas bubbles and in the bubble cap zone. From Fig. 9, it can

also be seen that for a given distance it is easier to approach the limitation of gas absorption for flow conditions with short slugs, which are more favorable for application design.

In this article, the effect of system pressure on the gas dissolution rate was investigated. Fig. 10(a) shows an example for the analysis of dissolving bubbles in the microchannel under system pressure up to 3.0 MPa with  $j_G=0.232$  m/s,  $j_L=0.116$  m/s. Despite the relatively larger deviation in the initial bubble lengths, the effect of system pressure on the gas dissolution rate can be roughly distinguished. That is, the dissolution rate increases with the increase of system pressure. To clarify this effect, the dissolution rate was normalized with  $L_{B0}-L_B$  at infinity to eliminate the distraction of initial bubble length and absorption capacity. The results are shown in Fig. 10(b). The effect of pressure is obvious as indicated. With gas bubbles moving downstream,  $L_{B0}-L_B$  approached the maximum value faster at higher system pressures. It indicates that absorption under elevated pressure would improve the reactor performance through increasing the absorption efficiency.

### 3.3. Mass transfer coefficients

As stated in Section 2.3, the volumetric mass transfer coefficients  $k_L a$  was obtained by fitting the bubble length with Eq. (4). Since the specific surface area  $a$  can be calculated based on the recorded images (Sobieszuk et al., 2011; Yao et al., 2013), liquid side mass transfer coefficient  $k_L$  was also obtained by dividing  $k_L a$  by  $a$ . Fig. 11(a) and (b) show the calculated  $k_L a$  under different system pressures at liquid flow rate 1.0 and 1.25 ml/min, respectively. And the corresponding values of  $k_L$  are shown in Fig. 12 (a) and (b). It shows that the tendency with phase flow rates under

each pressure condition is similar.  $k_L a$  increases either with increasing gas flow rate or liquid flow rate. The effect of liquid flow rate is larger than gas flow rate. Higher gas and liquid flow rates both lead to larger convective recirculation inside liquid slugs, but extra benefits for mass transfer with smaller bubble and slugs (Berčić and Pintar, 1997; Vandu et al., 2005; Yao et al., 2014b; Yue et al., 2009) are obtained when increasing liquid flow rates (Yao et al., 2014a, 2013).

The results in the present study indicate a positive effect of system pressure on the mass transfer. As shown in Figs. 11 and 12, a clear increase of mass transfer coefficient is observed when system pressure is elevated. As far as we know, the influence of system pressure on mass transfer in micro/mini channels has not been studied in literature before. But such studies in conventional columns or tanks have already been widely reported (Benadda et al., 1996; Letzel et al., 1999; Kojima et al., 1997; Maalej et al., 2003, 2001). These results show that the effect of system pressure on mass transfer is more related to the effect on the hydrodynamics, which is also true in microchannels. As is known that gas bubble in rectangular channels acts like a leaky piston, considerable amount of liquid bypasses the bubble through the channel corners (Harris Wong et al., 1995; Fuerstman et al., 2007). Therefore, for mass transfer in a unit cell, the mixing between the liquid in the slug and the liquid in the film is also very important compared to the convective mixing in the slug. Such factor sometimes may lead to a decrease in  $k_L$  (Fig. 12(a)) even when gas flow rate is increased and longer bubble is generated (Dietrich et al., 2013; Yao et al., 2014b). When the system pressure is elevated, the cross section of gas bubble increases, leading to less but faster-moving liquid existing in the channel corners and around bubble (Harris Wong et al., 1995; Yao et al., 2014a). This may be the reason for the increase in mass transfer coefficients given by the fact that

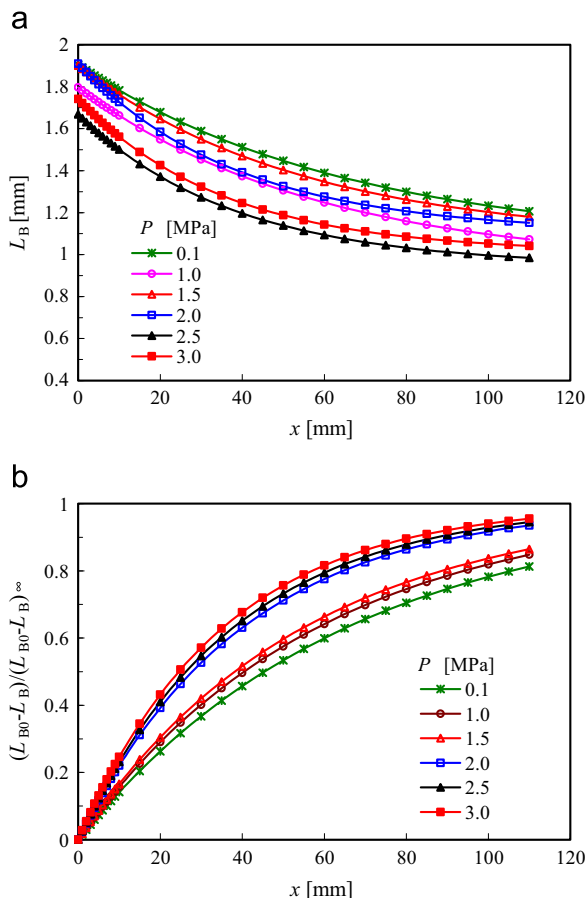


Fig. 10. (a) Bubble size and (b) normalized bubble size evolution versus  $x$  under different system pressures,  $j_G=0.232$  m/s,  $j_L=0.116$  m/s.

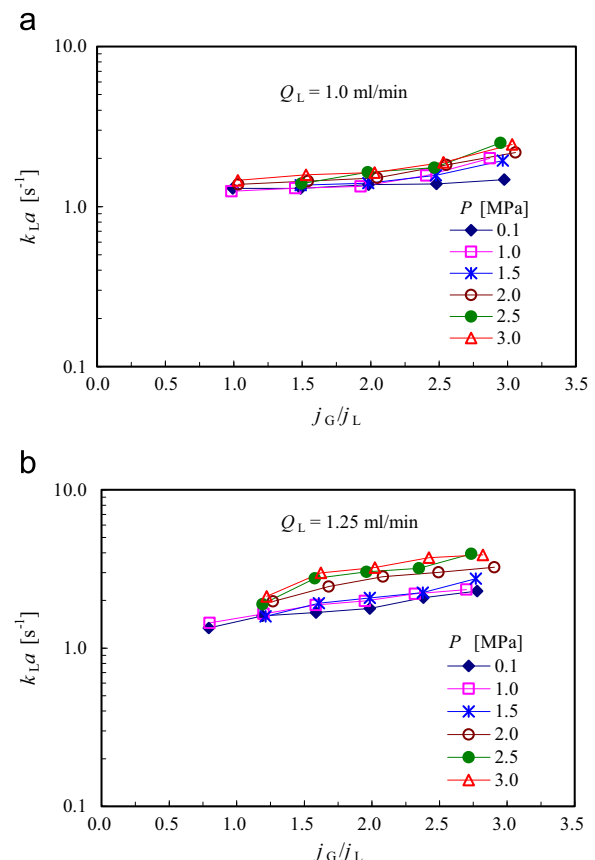


Fig. 11. The liquid side volumetric mass transfer coefficients  $k_L a$  under different system pressures.

the gas-liquid interfacial area is larger and the mixing between the liquid film and the liquid slug is faster. However, as the difference in hydrodynamics is relatively small, the enhancement of mass transfer is also limited to a certain extent, unlike the large effect reported in conventional tanks (Letzel et al., 1999; Kojima et al., 1997).

For the estimation of mass transfer coefficients under different pressures, an empirical correlation was proposed:

$$Sh_L ad_h = 0.094 Re_C^{0.0656} Re_L^{0.654} Sc_L^{1.449} Ca_{TP}^{0.839} \quad (8)$$

where all parameters are based on the inlet conditions. A total of 185 sets of experimental data were correlated with the current T-junction microchannel. The superficial velocities were in the range of  $0.08 < j_G < 0.51$  m/s;  $0.09 < j_L < 0.19$  m/s. A good prediction performance is obtained, as shown in Fig. 13.

### 3.4. Gas absorption during bubble formation

Mass transfer during the gas bubble formation is very important in several aspects such as reactor evaluation (Sobieszuk et al., 2011; Yue et al., 2007), fundamental study (Ganapathy et al., 2013; Tan et al., 2012) and new application field development (Lefortier et al., 2012; Li et al., 2012). However, there were very few studies focused on this area and they only emerged in the recent years. Tan et al. (2012) measured the CO<sub>2</sub> concentration in the gas bubbles after the formation stage by comparing the bubble length at this stage and at the outlet, where CO<sub>2</sub> was assumed to be completely exhausted and only N<sub>2</sub> was left. They found a fraction of about 30% of CO<sub>2</sub> to be absorbed by NaOH solutions. A numerical simulation of gas-liquid mass transfer during bubble formation was conducted by Ganapathy et al. (2013). With low CO<sub>2</sub> and NaOH concentration, the absorption fraction in the inlet

mixing region was generally smaller than 10% for various channel diameters. It is note-worthy that their prediction showed that for a given residence time, a smaller absorption fraction was observed when inlet mass transfer during bubble formation was modeled than not. It suggests the liquid side volumetric mass transfer coefficient  $k_L a$  during bubble formation may be smaller than that during bubble flowing in the main channel.

In this work, the amount of gas absorption during bubble formation is defined as the bubble size reduction in this duration. By assuming that  $k_L a$  during the formation stage is equal to that in the main channel, the bubble length right at the T-junction  $L_{B0}$  can be extrapolated with Eq. (4). The absorption fraction is then calculated as

$$\varphi = \frac{1 - L_B(x_1)}{L_{B0}} \quad (9)$$

$$x_1 = \frac{U_{B0}}{f} \quad (10)$$

where  $x_1$  is the mass transfer distance during formation process and  $\varphi$  means the fraction of gas absorbed in the feeding gas. The calculated  $L_B(x_1)$  equals the initially generated bubble length  $L_{B1}$  determined from the captured images, but the method offers a convenient way to predict  $L_{B1}$ . The results are plotted in Fig. 14. Under experimental conditions, the fraction  $\varphi$  varies from 1.5% to 4% of the feeding gas, which corresponded to 3% to 8% of the absorption capacity of the feeding liquid. Our results here were much lower than the results reported by (Tan et al., 2012), but very

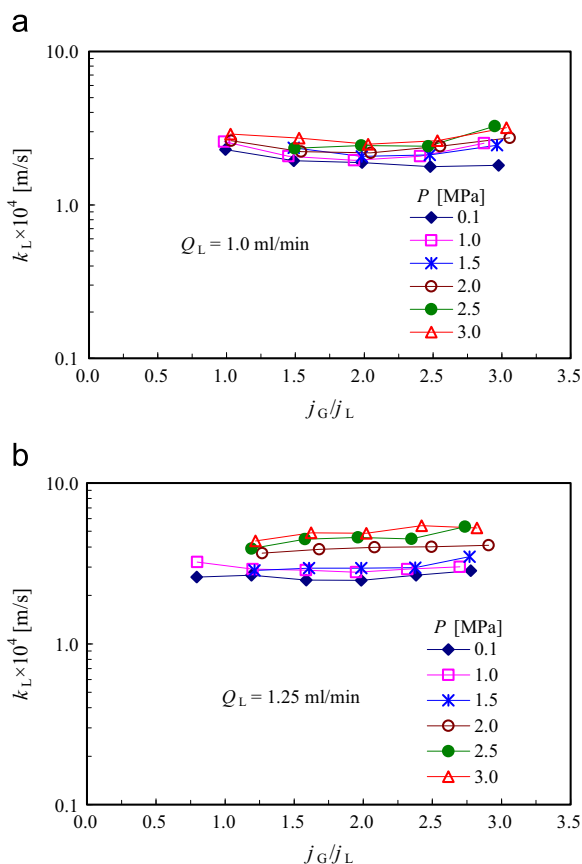


Fig. 12. The liquid side mass transfer coefficients  $k_L$  under different system pressures.

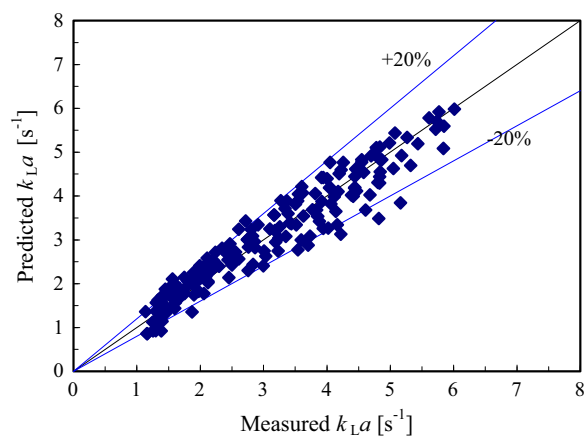


Fig. 13. Comparison between the measured and predicted values of  $k_L a$  with Eq. (8).

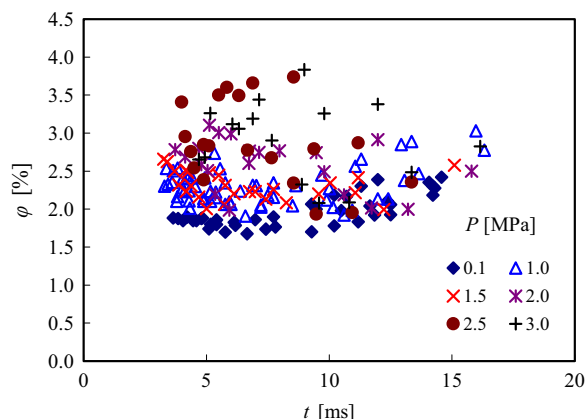


Fig. 14. The fraction of gas absorbed during the bubble formation as a function of the formation period.

close to the results of Ganapathy et al. (2013). In fact,  $\varphi$  was closely related to three factors, mass transfer rate, gas solubility and bubble formation period (Yao et al., 2014b). For short duration, mass transfer during the stage can be treated as constant at the largest transfer rate. A linear relationship was found between  $\varphi$  and  $k_L a C^* t$  (Yao et al., 2014b). The relationship explained the discrepancy between our results and Tan et al. (2012). Because their formation time was 20 to 40 times larger than ours and the chemical reaction largely enhanced the absorption rate. It also explained the effect of system pressure on the absorption during formation shown in Fig. 14. As mass transfer coefficients are larger at higher pressure,  $\varphi$  increases with the increase in system pressure. This also explains the fact that smaller gas bubbles are generated at higher system pressure.

#### 4. Conclusion

This article reports a study of gas-liquid flow and mass transfer in a microchannel with T-junction under elevated system pressures. Visualization experiments were carried out to study the bubble and slug length and bubble size evolution along the channel length. Mass transfer coefficients were calculated with a unit cell model (Yao et al., 2014b), which was based on the rate of bubble size reduction. The effect of system pressure on flow and mass transfer was investigated. The findings can be served as guidance in designing high pressure gas-liquid microreactors.

It has been found that increasing the system pressure of CO<sub>2</sub>-water tends to generate smaller gas bubbles while the effect on liquid slug is not obvious. However, the ratio of bubble length to unit cell length decreases with the increase in system pressure for a given injection volume fraction. It corresponds with previous results that the bubble cross-sectional area is increased when system pressure is elevated (Yao et al., 2014a). Another contribution to this fact is that more gas was absorbed during bubble formation at higher system pressure. The fraction of gas absorbed during the bubble formation only accounts for 1.5% to 4.0% of the inlet feeding gas phase. The bubble size reduction was used to evaluate the mass transfer. At a constant system pressure, the difference in the reduction rate varies very little for short contact distances. But the final reduction of the bubble size only depends on the liquid amount in single unit cell, resulting in lower gas bubble dissolution rate with shorter liquid slugs. For various system pressures, a significant influence of system pressure was observed. Higher mass transfer coefficients were obtained when system pressure was elevated. An empirical correlation was proposed to estimate the liquid-phase volumetric mass transfer coefficient under experimental conditions with good fitting performance. This article only presents experimental results and further studies that explore more fundamental transport behavior will be required.

#### Nomenclature

$a$	specific surface area, m <sup>2</sup> /m <sup>3</sup>
$A$	cross-sectional area, m <sup>2</sup>
$C$	CO <sub>2</sub> concentration in water, mol/L
$C^*$	physical solubility of CO <sub>2</sub> in water, mol/L
$Ca_{TP}$	two phase capillary number defined by ( $=\mu_L j_{TP}/\sigma_L$ ), dimensionless
$D_H$	Hydrodynamic diameter, $\mu\text{m}$
$f$	Bubble formation frequency, Hz
$j$	superficial velocity, m/s
$k_L$	liquid side mass transfer coefficient, m/s
$k_L a$	liquid side volumetric mass transfer coefficient, s <sup>-1</sup>

$m$	parameters in Eq.(4)
$t$	time, s
$L$	length
$P$	pressure
$P_a$	atmospheric pressure
$Q$	flow rates, mL/min
$R$	gas constant, 8.3145 J/(K · mol)
$Re_G$	superficial gas Reynolds number defined by ( $=D_H j_G \rho_G / \mu_G$ )
$Re_L$	superficial liquid Reynolds number defined by ( $=D_H j_L \rho_L / \mu_L$ )
$Sc_L$	liquid Schmidt number defined by ( $=\mu_L / \rho_L D$ )
$Sh_L$	liquid Sherwood number defined by ( $=k_L D_H / D$ )
$T$	temperature, K
$U$	velocity, m/s
$V$	volume, mL
$W$	channel width
$x$	distance from the T-junction, mm

#### Subscripts

B	bubble
B0	extrapolated bubble length at the T-junction.
B1	the initial generated bubble
G	gas
L	liquid
S	liquid slug

#### Acknowledgments

We acknowledge gratefully the financial supports for this project from National Natural Science Foundation of China (Nos. 21225627, 21376234, 91334201).

#### References

- Berčić, G., Pintar, A., 1997. The role of gas bubbles and liquid slug lengths on mass transport in the Taylor flow through capillaries. *Chem. Eng. Sci.* 52, 3709–3719.
- Bennada, B., Otterbein, M., Kafoufi, K., Prost, M., 1996. Influence of pressure on the gas-liquid interfacial area and the coefficient  $k_L a$  in a counter-current packed column. *Chem. Eng. Process.* 35, 247–253.
- Chao, H., Chen, G., Yuan, Q., 2009. Testing and design of a microchannel heat exchanger with multiple plates. *Ind. Eng. Chem. Res.* 48 (9), 4535–4541.
- Chao, H., Chen, G., Yuan, Q., 2010. Thermal performance of crossflow microchannel heat exchangers. *Ind. Eng. Chem. Res.* 49 (13), 6215–6220.
- Chen, G., Yue, J., Yuan, Q., 2008. Gas-liquid microreaction technology: recent developments and future challenges. *Chinese J. Chem. Eng.* 16, 663–669.
- Dietrich, N., Loubière, K., Jimenez, M., Hébrard, G., Gourdon, C., 2013. A new direct technique for visualizing and measuring gas-liquid mass transfer around bubbles moving in a straight millimetric square channel. *Chem. Eng. Sci.* 100, 172–182.
- Fuerstman, M.J., Lai, A., Thurlow, M.E., Shevkoplyas, S.S., Stone, H.A., Whitesides, G.M., 2007. The pressure drop along rectangular microchannels containing bubbles. *Lab Chip* 7, 1479–1489.
- Ganapathy, H., Al-Hajri, E., Ohadi, M., 2013. Mass transfer characteristics of gas-liquid absorption during Taylor flow in mini/microchannel reactors. *Chem. Eng. Sci.* 101, 69–80.
- Garstecki, P., Fuerstman, M.J., Stone, H.A., Whitesides, G.M., 2006. Formation of droplets and bubbles in a microfluidic T-junction—scaling and mechanism of break-up. *Lab Chip* 6, 437–446.
- Guo, F., Chen, B., 2009. Numerical study on Taylor bubble formation in a micro-channel T-junction using VOF method. *Microgravity Sci. Tech.* 21, 51–58.
- Hessel, V., Angeli, P., Gavrilidis, A., Löwe, H., 2005. Gas-liquid and gas-liquid-solid microstructured reactors contacting principles and applications. *Ind. Eng. Chem. Res.* 44, 9750–9769.
- Jensen, K.F., 2001. Microreaction engineering – is small better? *Chem. Eng. Sci.* 56, 293–303.
- Kojima, H., Sawai, J., Suzuki, H., 1997. Effect of pressure on volumetric mass transfer coefficient and gas holdup in bubble column. *Chem. Eng. Sci.* 52, 4111–4116.
- Keybl, J., Jensen, K.F., 2011. Microreactor system for high-pressure continuous flow homogeneous catalysis measurements. *Ind. Eng. Chem. Res.* 50, 11013–11022.
- Letzel, H.M., Schouten, J.C., Krishna, R., van den Bleek, C.M., 1999. Gas holdup and mass transfer in bubble column reactors operated at elevated pressure. *Chem. Eng. Sci.* 54, 2237–2246.

- Lefortier, S.G.R., Hamersma, P.J., Bardow, A., Kreutzer, M.T., 2012. Rapid microfluidic screening of CO<sub>2</sub> solubility and diffusion in pure and mixed solvents. *Lab Chip* 12, 3387–3391.
- Li, W., Liu, K., Simms, R., Greener, J., Jagadeesan, D., Pinto, S., Gunther, A., Kumacheva, E., 2012. Microfluidic study of fast gas-liquid reactions. *J. Am. Chem. Soc.* 134, 3127–3132.
- Maalej, S., Benadda, B., Otterbein, M., 2003. Interfacial area and volumetric mass transfer coefficient in a bubble reactor at elevated pressures. *Chem. Eng. Sci.* 58, 2365–2376.
- Maalej, S., Benadda, B., Otterbein, M., 2001. Influence of pressure on the hydrodynamics and mass transfer parameters of an agitated bubble reactor. *Chem. Eng. J.* 24, 77–84.
- Marre, S., Adamo, A., Basak, S., Aymonier, C., Jensen, K.F., 2010. Design and packaging of microreactors for high pressure and high temperature applications. *Ind. Eng. Chem. Res.* 49, 11310–11320.
- Muradoglu, M., 2010. Axial dispersion in segmented gas-liquid flow: effects of alternating channel curvature. *Phys. Fluids* 22, 122106.
- Nielsen, L.C., Bourg, I.C., Sposito, G., 2012. Predicting CO<sub>2</sub>-water interfacial tension under pressure and temperature conditions of geologic CO<sub>2</sub> storage. *Geochim. Cosmochim. Ac.* 81, 28–38.
- Pohorecki, R., 2007. Effectiveness of interfacial area for mass transfer in two-phase flow in microreactors. *Chem. Eng. Sci.* 62, 6495–6498.
- Shao, N., Gavriilidis, A., Angeli, P., 2009. Flow regimes for adiabatic gas-liquid flow in microchannels. *Chem. Eng. Sci.* 64, 2749–2761.
- Sobieszuk, P., Aubin, J., Pohorecki, R., 2012. Hydrodynamics and mass transfer in gas-liquid flows in microreactors. *Chem. Eng. Tech* 35, 1346–1358.
- Sobieszuk, P., Pohorecki, R., Cygański, P., Grzelka, J., 2011. Determination of the interfacial area and mass transfer coefficients in the Taylor gas-liquid flow in a microchannel. *Chem. Eng. Sci.* 66, 6048–6056.
- Su, Y., Chen, G., Zhao, Y., Yuan, Q., 2009. Intensification of liquid-liquid two-phase mass transfer by gas agitation in a microchannel. *AIChE J* 55, 1948–1958.
- Tan, J., Lu, Y.C., Xu, J.H., Luo, G.S., 2012. Mass transfer characteristic in the formation stage of gas-liquid segmented flow in microchannel. *Chem. Eng. J.* 185–186, 314–320.
- Trachsel, F., Hutter, C., Vonrohr, P., 2008. Transparent silicon/glass microreactor for high-pressure and high-temperature reactions. *Chem. Eng. J.* 135, S309–S316.
- Triplett, K.A., Ghiaasiaan, S.M., Abdel-Khalik, S.I., Sadowski, D.L., 1999. Gas-liquid two-phase flow in microchannels – part I: two-phase flow patterns. *Int. J. Multiph. Flow* 25, 377–394.
- Vandu, C.O., Liu, H., Krishna, R., 2005. Mass transfer from Taylor bubbles rising in single capillaries. *Chem. Eng. Sci.* 60, 6430–6437.
- Verboom, W., 2009. Selected examples of high-pressure reactions in glass microreactors. *Chem. Eng. Tech* 32, 1695–1701.
- Wong, Radke, C.J., Morris, S., 1995. The motion of long bubbles in polygonal capillaries. Part 2. Drag, fluid pressure and fluid flow. *J. Fluid Mech.* 292, 95–100.
- Yao, C., Dong, Z., Zhao, Y., Chen, G., 2014a. The effect of system pressure on gas-liquid slug flow in a microchannel. *AIChE J* 60, 1132–1142.
- Yao, C., Dong, Z., Zhao, Y., Chen, G., 2014b. An online method to measure mass transfer of slug flow in a microchannel. *Chem. Eng. Sci.* 112, 15–24.
- Yao, C., Zhao, Y., Ye, C., Dang, M., Dong, Z., Guangwen, C., 2013. Characteristics of slug flow with inertial effects in a rectangular microchannel. *Chem. Eng. Sci.* 95, 246–256.
- Ye, C., Dang, M., Yao, C., Chen, G., Yuan, Q., 2013. Process analysis on CO<sub>2</sub> absorption by monoethanolamine solutions in microchannel reactors. *Chem. Eng. J.* 225, 120–127.
- Yue, J., Chen, G., Yuan, Q., Luo, L., Gonthier, Y., 2007. Hydrodynamics and mass transfer characteristics in gas-liquid flow through a rectangular microchannel. *Chem. Eng. Sci.* 62, 2096–2108.
- Yue, J., Luo, L., Gonthier, Y., Chen, G., Yuan, Q., 2009. An experimental study of air-water Taylor flow and mass transfer inside square microchannels. *Chem. Eng. Sci.* 64, 3697–3708.
- Zaloha, P., Kristal, J., Jiricny, V., Völkel, N., Xuereb, C., Aubin, J., 2012. Characteristics of liquid slugs in gas-liquid Taylor flow in microchannels. *Chem. Eng. Sci.* 68, 640–649.
- Zhao, Y., Chen, G., Ye, C., Yuan, Q., 2013a. Gas-liquid two-phase flow in microchannel at elevated pressure. *Chem. Eng. Sci.* 87, 122–132.
- Zhao, Y., Yao, C., Chen, G., Yuan, Q., 2013b. Highly efficient synthesis of cyclic carbonate with CO<sub>2</sub> catalyzed by ionic liquid in a microreactor. *Green Chem.* 15, 446–452.
- de Menech, M., Garstecki, P., Jousse, F., Stone, H.A., 2008. Transition from squeezing to dripping in a microfluidic T-shaped junction. *J. Fluid Mech.* 595, 141–146.
- dos Santos, A.P., Levin, Y., 2010. Surface tensions and surface potentials of acid solutions. *J. Chem. Phys.* 133, 154107.
- van Baten, J.M., Krishna, R., 2004. CFD simulations of mass transfer from Taylor bubbles rising in circular capillaries. *Chem. Eng. Sci.* 59, 2535–2545.
- van Steijn, V., Kreutzer, M.T., Kleijn, C.R., 2007.  $\mu$ -PIV study of the formation of segmented flow in microfluidic T-junctions. *Chem. Eng. Sci.* 62, 7505–7514.